

THE TURBULENT SHEAR STRESS AND TURBULENT HEAT FLUX OF TWO PARALLEL PLANE JETS WITH PERIODIC VORTEX SHEDDING

Soichiro Hiromasa

Department of Mechanical Engineering
Doshisha University
1-3 Tatara Miyakodani, Kyotanabe-shi, Kyoto, Japan,
ctwg0515@mail4.doshisha.ac.jp

Shumpei Hara

Department of Mechanical Science Engineering
Doshisha University
1-3 Tatara Miyakodani, Kyotanabe-shi, Kyoto, Japan,
shhara@mail.doshisha.ac.jp

Kyoji Inaoka

Department of Mechanical and System Engineering
Doshisha University
1-3 Tatara Miyakodani, Kyotanabe-shi, Kyoto, Japan,
kinaoka@mail.doshisha.ac.jp

ABSTRACT

The turbulent velocity and heat flux of two parallel plane jets with a periodic vortex shedding phenomenon were experimentally investigated using simultaneous particle imaging velocimetry and two-color laser induced fluorescence. In the upstream regions, the incoming jet feeds the recirculation zone, causing the temperature to stay constant, leading to small turbulent heat flux. For jets with a nozzle distance ratio of 1.4, the vortex shedding phenomenon suppresses the inner shear layers, causing both Reynolds shear stress and turbulent heat flux within this region to become smaller in comparison to two parallel plane jets without a periodic vortex shedding. However, these vortices also stimulate the outer shear layers, causing turbulent statistics to spread greater in the transverse direction.

INTRODUCTION

Thermal pollution caused by thermal discharge from plants and stack gas ravage the ecosystem, and turbulent diffusion from jets shines light in ways to lessen the damage caused. One way to improve turbulent diffusion in jets is by using two parallel plane jets. Tanaka (1970, 1974) experimented by changing the distance ratio between jets and compared the results to a single jet, concluding that two parallel plane jets had active diffusion characteristics, while also stating that the distance ratio d/w (d being the distance between the two jets and w being the width of each jet) affects the flow field greatly, with different phenomenon occurring between the jets according to the distance ratio. Bunderson and Smith (2005) reported vortices forming and wavering within the recirculation zone, while Anderson et al. (2003) reported a vortex shedding phenomenon occurring when the distance ratio is between 0.6 and 1.4, which was confirmed by Mondal et al. (2016) through numerical simulation. The effects of the vortex shedding phenomenon upon vector values have been studied upon, yet scalar values such as temperature have been paid little attention. Throughout inspection of previous studies, signs indicate active turbulent diffusion in two parallel plane jets and values. However, in order to fully incorporate two parallel plane jets into industrial usage, heat transfer must

be studied and evaluated upon.

The purpose of the present study is to measure the turbulent velocity and turbulent heat flux of two parallel plane jets using simultaneous particle imaging velocimetry (PIV) and two-color laser induced fluorescence (LIF) method. By evaluating vector values and scalar values, quantitative insight on turbulent velocity and turbulent heat flux for jets with or without a periodic vortex shedding phenomenon is presented.

EXPERIMENT APPARATUS AND PROCEDURE

The flow system is shown in Fig. 1, done in an acrylic water tank ($800 \times 500 \times 1000$ mm³). Two side plates along the nozzle were used to retain the two-dimensionality of the jet and two rectangular exits were placed parallel to each other. Each exit had a width of $w = 3$ mm and length $l = 60$ mm (an aspect ratio of 20). The distance between the two nozzles were $d = 4.2$ mm and $d = 6.0$ mm for case 1 and case 2 respectively, shown in the schematic view of the test section in Fig. 2. A Cartesian coordinate system was established, with its origin located at the center of the two nozzles with the vertical direction the x -axis and the horizontal direction the y -axis, with the x component velocity and y component velocity noted as u and v . The exit Reynolds number ($Re_0 \equiv U_0 w / \nu$) were 810 and 890 for case 1 and case 2, U_0 being the average exit u velocity and ν the kinematic viscosity of water. The development of two parallel plane jets can be divided into 3 regions (Miller and Comings, 1960). The converging region (region A) consists of a recirculation zone bordered by the two jets which continues until where the two jets meet at the centerline known as the merging point (mp). The region between mp and where the two jets form a velocity distribution of a single jet (combined point, cp) is the merging region (region B), and any region downstream of this point is considered the combined region (region C). A 10 degree temperature difference was also implemented between the jet exit and surrounding fluid.

The measurement system used for the simultaneous PIV and two-color LIF measurements is shown in Fig. 3. A laser with a wavelength of 488 nm was used, and the emitted beam was adjusted using multiple mirrors and made into a 2 mm

laser sheet using a pinhole and a cylindrical lens. From one side of the water tank, PIV measurements were obtained using a CCD camera (800 fps, pixel resolution of 640×480 pixels, spatial resolution of 0.166 mm/pixel), to track the $50 \mu\text{m}$ nylon particles dispersed throughout the tank. Two-color LIF measurements were made using Rhodamine B (RhB) and Rhodamine 110 (Rh110) circulating throughout the flow system. Two CMOS cameras with a pixel resolution of 564×480 pixels and a spatial resolution of 0.166 mm/pixel were used at 400 fps for LIF measurements. A dichroic mirror was used to obtain identical areas of measurements for the two LIF cameras, placed at the opposite side of the tank from the PIV camera. Filters were used for each CMOS cameras to allow different wavelengths to enter each camera. Wavelengths between 495 nm and 530 nm were allowed to enter the CMOS camera for Rh110 measurements, and wavelengths above 570 nm entered cameras for RhB measurements. Simultaneous measurements were conducted for 15 seconds, and calculations to obtain temperature values were done using methods used by Sakakibara and Adrian (1999). A calibration test was done in a test-cell by taking a sample of the RhB and Rh110 solution and heating up the solution from 25 degrees to 35 degrees. A second degree calibration curve was obtained from the fluorescence ratio of two LIF images taken at every 0.5°C and the solution's temperature obtained by a thermocouple, measurement errors related to calibration not expected to exceed $5.3\%/^\circ\text{C}$.

RESULTS AND DISCUSSION

Time Averaged Statistics

The velocity field of the two cases are shown in Fig. 4, with lines at the merging point (*mp*) and combined point (*cp*) for each case. The *mp* and *cp* were located at $x/w = 1.3$ and $x/w = 5.0$ for case 1 and $x/w = 2.0$ and $x/w = 5.9$ for case 2. With the locations of the *mp* for case 1 and case 2 being similar to the points found in previous studies (Lee et al. (2018), Wang et al. (2015)), it is safe to assume that the *mp* moves downstream along with the distance ratio.

Temperature differences between the jet and surrounding fluid are shown in Fig. 5, made dimensionless with the temperature difference between the jet exit and surrounding fluid. For both cases, the recirculation zone has a constant temperature distribution regardless of the backwards flow. Due to the fluids in the recirculation zone being supplied by the incoming high temperature jets, the average temperature remains constant. The temperature begins to decline in the streamwise direction and transverse direction in Region B for both cases, as entrainment of the surrounding fluid causes the temperature difference to become smaller.

Figure 6 shows the dimensionless mean Reynolds shear stress for either case, with the black dotted lines representing the shear layers. These shear layers were determined as locations with at least 2 percent of the maximum Reynolds shear stress of the entire field of measurement. Inner shear layers are caused by the interaction between the individual jets while merging, and with the *mp* being located closer for case 1, the merging of the jets occurs more upstream, leading to smaller inner shear layers. When comparing the Reynolds shear stress along the *mp* for each case, peak values in the inner shear layers were found to be approximately 2.5 times that of the peak values of the outer shear layers for both cases. Although there is turbulent mixing occurring with the surrounding fluid in the outer shear layers, the merging of the jets produces higher turbulence, hence taking a larger value.

The time-averaged transverse turbulent heat flux for both cases are shown in Fig. 7. Values are made dimensionless using U_0 and ΔT_0 , which are the exit velocity and the temperature difference between the jet exit and surrounding fluid. In both cases, region A showed little turbulent heat flux, not in alignment with observations for Reynolds shear stress. The discrepancy is that Reynolds shear stress is a product of two velocity vectors while turbulent heat flux is a product of a velocity vector and a temperature scalar. As shown in Fig. 5, high temperature fluids keeps on recirculating within region A from the incoming jet and is able to retain a constant temperature, resulting in small turbulent heat flux. In region B and region C, the time-varying component of temperature (t') becomes larger as heat is not constantly fed into the region, causing an increase in turbulent heat flux. Transverse turbulence is also a cause, as the merging of the two jets causes v' to become larger, leading to greater turbulent heat flux when compared to region A. A difference that can be seen between the two cases is that case 1 shows a greater spread in turbulent heat flux when compared to case 2, which will be discussed later on.

Instantaneous and Phase Averaged Statistics

To grasp the differences in flow structures between the two cases, the instantaneous velocity streamlines for case 1 and case 2 are shown in Fig. 8. For either case, two vortices are present within the recirculation zone, but their location and movement differ between cases. For case 1, counter rotating vortices are present in the top left and bottom right of the recirculation zone, while being aligned next to each other at times for case 2, similar to the findings of previous research (Mondal et al., 2016). To confirm a periodic vortex shedding for case 1, the Fast Fourier Transform (FFT) was performed with v' at $(x/w, y/w) = (mp, 0.5 (d/w)) = (1.3, 0.7)$, where neither the streamwise nor transverse velocity is dominant. A peak frequency of $f = 15.6$ Hz was obtained and converted into a Strouhal number $St (\equiv fd/U_0) = 0.33$, in line with results previous experimental results (Anderson et al., 2003). Although vortices were shed at times for case 2, FFT showed no periodic vortex shedding frequency.

Using this frequency, phase averaging was carried out and four phases within a time period were created for case 1. The streamlines of the phase averaged results are shown in Fig. 9, with results similar to the instantaneous results. Vortices were shown to not align with each other and vortices are shown to oscillate one after another. The first phase in Fig. 9 (a) shows the vortex on the right downstream while the vortex on the left is forming. Figure 9 (b) has a vortex forming on the right being shed while a vortex on the left is developing. Afterwards, the vortex on the right begins to form while the vortex on the left moves downstream in Fig. 9 (c). Finally, the vortex on the right enlarges and the vortex on the left is shed in Fig. 9 (d). It must be noted that just past the merging point along the jet centerline at $x/w = 1.9$, the jet is seen to waver in the transverse direction in a periodic fashion. A peak frequency of $f = 15.6$ Hz was at this point as well, showing that the periodic vortex shedding plays a key role in the jet wavering in downstream regions.

Totaled Turbulent Statistics

The total magnitude of Reynolds shear stress across each cross section for inner and outer shear layers are plotted in Fig. 10, with areas of each shear layer determined as previously mentioned. The total amount of Reynolds shear stress in the inner shear region for each cross-section is plotted in Fig. 10 (a), showing that both cases show similar trends, tak-

ing a peak value at the mp and declining rapidly afterwards. The effects of the periodic vortex shedding becomes evident in the outer shear layers, plotted in Fig. 10 (b). Similar trends are apparent in region (A), with the increase in total Reynolds shear stress coming to a halt once past the mp . In the instance of case 2, Reynolds shear stress totals decrease until $x/w = 4.6$ where the total values begin to increase again. However, for case 1, Reynolds shear stress totals decrease only up until $x/w = 2.0$, where these values begin to increase again. The periodic vortex shedding for case 1 plays a key role in destabilizing the outer shear layers (Mondal et al. 2016), as the vortex shedding creates a periodic wavering at $x/w = 1.9$, leading to the destabilization of the outer shear layers. This destabilization allows for greater momentum transfer to occur in downstream regions when compared to case 2.

Similar to the total Reynolds shear stress, the total turbulent heat flux values in the shear layers showed signs of the effects of the periodic vortex shedding as well, shown in Fig. 11. In the inner shear layers shown in Fig. 11 (a), similar turbulent heat flux totals are shown until $x/w = 2.0$. From this point where turbulent heat flux becomes relatively constant for case 1. For case 2, total turbulent heat flux values continue to increase until $x/w = 2.8$ where turbulent heat flux becomes relatively constant. In both cases, turbulent heat flux becomes smaller as the shear layers shrinks in size, starting at $x/w = 3.1$ for case 1 and $x/w = 3.9$ for case 2. When observing the outer shear layers in Fig. 11 (b), the inclination of total turbulent heat flux remains relatively constant in the downstream regions for case 1. However, case 2 shows turbulent heat flux rise rapidly until $x/w = 3.9$ where its slope becomes relatively smaller. The constant destabilization of the outer shear regions for case 1 causes the transverse direction velocity fluctuations to spread as well, hence greater total values.

To address how the turbulent statistics spread, the slopes of the half widths of Reynolds shear stress ($C_{1u'v'}$) and turbulent heat flux ($C_{1v't'}$) were obtained using equation (1) and equation (2).

$$b_{u'v'}/w = C_{1u'v'}(x/w + C_{2u'v'}) \quad (1)$$

$$b_{v't'}/w = C_{1v't'}(x/w + C_{2v't'}) \quad (2)$$

Locations where Reynolds shear stress and turbulent heat flux reached half the value of their local maximum values ($b_{u'v'}/w$ and $b_{v't'}/w$) were plotted using experimental data and linear approximation was used to obtain the slope of the half widths in the downstream direction ($C_{2u'v'}$, $C_{2v't'}$ being experimental constants). The slopes for both statistics are listed in Table 1, where the spreading of Reynolds shear stress and turbulent heat flux is found to be greater for case 1. To compare the spreading of Reynolds shear stress and turbulent heat transfer, a transport spreading coefficient CT , similar to the spreading coefficient that compared velocity half width slopes and temperature half width slopes (Jenkins and Goldschmidt, 1973) were obtained as shown in equation (3), with results listed in Table 1.

$$CT = C_{1v't'}/C_{1u'v'} \quad (3)$$

Through examination of $C_{1u'v'}$ and $C_{1v't'}$, the spread of Reynolds shear stress and turbulent heat flux is greater for case 1. With the periodic vortex shedding, a periodic disruption of the outer shear layers leads to a greater spread in turbulent statistics. The transfer coefficient CT shows that in both cases, the spread of Reynolds shear stress is greater than the spread of turbulent heat flux. Also, the spreading rate of turbu-

Table 1. Half width slopes based off Reynolds shear stress, turbulent heat flux and values of transport spreading coefficient.

Case	$C_{1u'v'}$	$C_{1v't'}$	CT
Case 1	0.33	0.22	0.67
Case 2	0.27	0.12	0.44

lent heat flux in comparison to Reynolds shear stress is greater for jets with a periodic vortex shedding.

CONCLUSION

Simultaneous PIV and two-color LIF were used to measure the turbulent velocity and turbulent heat flux of two parallel plane jets with different distance ratios. Jets with a periodic vortex shedding phenomenon were found to repress the inner shear layers while also stimulating outer shear layers. These effects are evident when comparing turbulent statistics to jets without a periodic vortex shedding, as the inner shear layers had smaller total Reynolds shear stress and turbulent heat flux. On the other hand, outer shear layers showed these jets to have higher total turbulent statistics. The half width slopes of turbulent statistics also showed that jets with a periodic vortex shedding have a greater rate of spreading when compared to jets without a periodic vortex shedding.

REFERENCES

- Anderson, E. A., Snyder D. O. & Christensen, J. 2003 Periodic flow between low aspect ratio parallel jets. *Journal of Fluids Engineering* **125** (2), 389–392.
- Bunderson, N.E. & Smith 2005 Passive mixing control of plane parallel jets. *Experiments in Fluids* **39**, 66–74.
- Jenkins, P.E., Goldschmidt V.W. 1973 Mean temperature and velocity in a plane turbulent jet. *Journal of Fluids Engineering* **95** (4), 581–584.
- Lee, Saya & Hassan, Yassin A. 2018 Experimental study of flow structures near the merging point of two parallel plane jets using piv and pod. *International Journal of Heat and Mass Transfer* **116**, 871–888.
- Miller, D.R., Comings E.W. 1960 Force-momentum fields in a dual-jet flow. *Journal of Fluid Mechanics* **7** (2), 237–256.
- Mondal, T., Das M. K. & Guha, A. 2016 Periodic vortex shedding phenomenon for various separation distances between two parallel plane jets. *International Journal of Heat and Mass Transfer* **99**, 579–588.
- Sakakibara, J. & Adrian, R.J. 1999 Whole field measurements of temperature in water using two-color laser induced fluorescence. *Experiments in Fluids* **26**, 7–15.
- Tanaka, Eiichi 1970 The interference of two-dimensional parallel jets : 1st report, experiments on dual jet. *Bulletin of JSME* **13**, 272–280.
- Tanaka, Eiichi 1974 The interference of two-dimensional parallel jets : 2nd report, experiments on the combined flow of dual jet. *Bulletin of JSME* **17** (109), 920–927.
- Wang, Huhu, Lee, Saya, Hassan, Yassin A. & Ruggles, Arthur Elwood 2016 Laser-doppler measurements of the turbulent mixing of two rectangular water jets impinging on a stationary pool. *International Journal of Heat and Mass Transfer* **92**, 206–227.

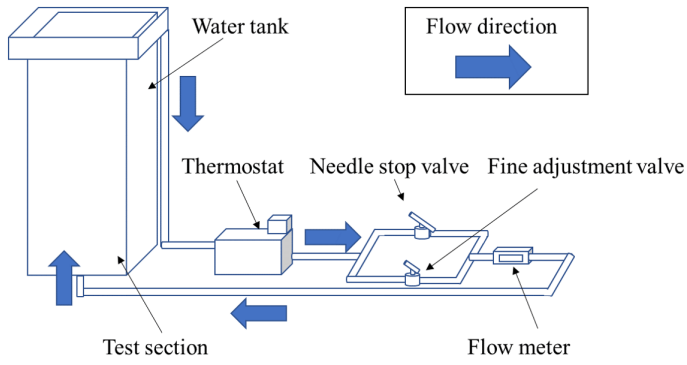


Figure 1. Flow system used throughout the experiment.

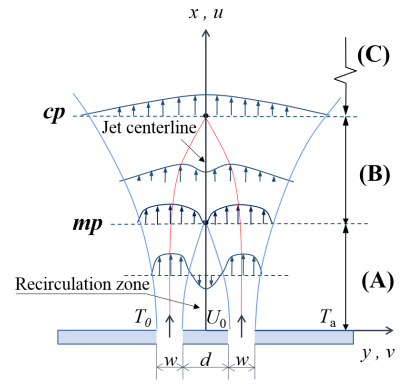


Figure 2. Schematic diagram of the flow field of two parallel plane jets.

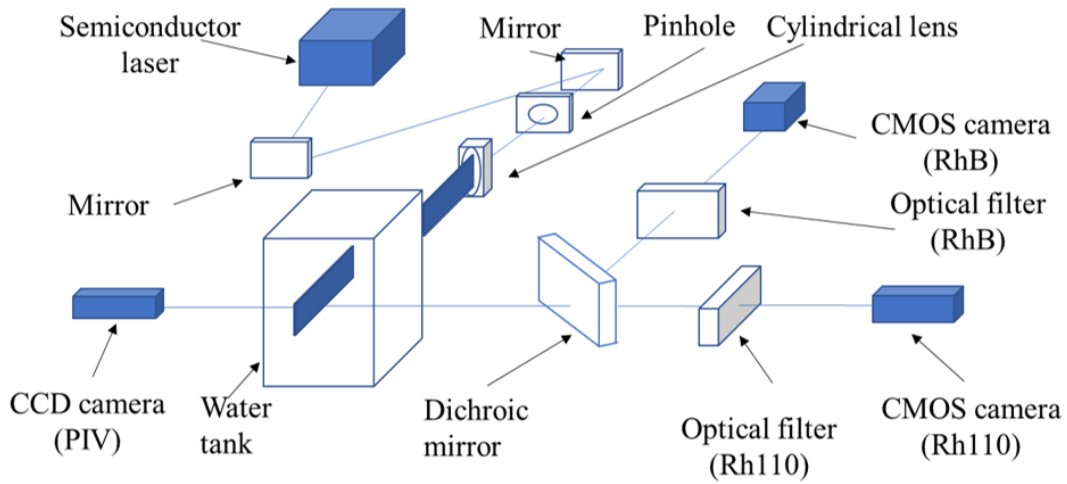


Figure 3. Simultaneous PIV and two-color LIF measurement system.

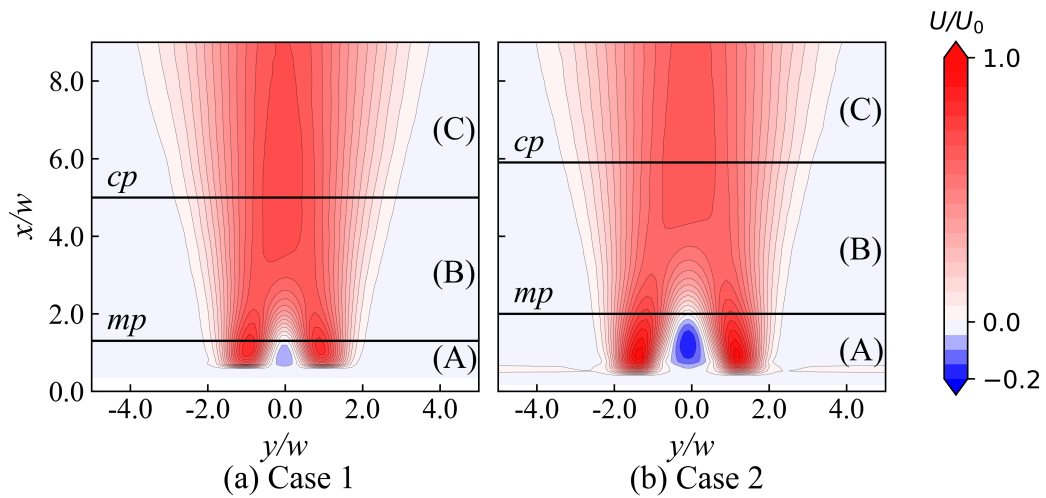


Figure 4. Dimensionless mean streamwise velocity for (a) case 1 and (b) case 2.

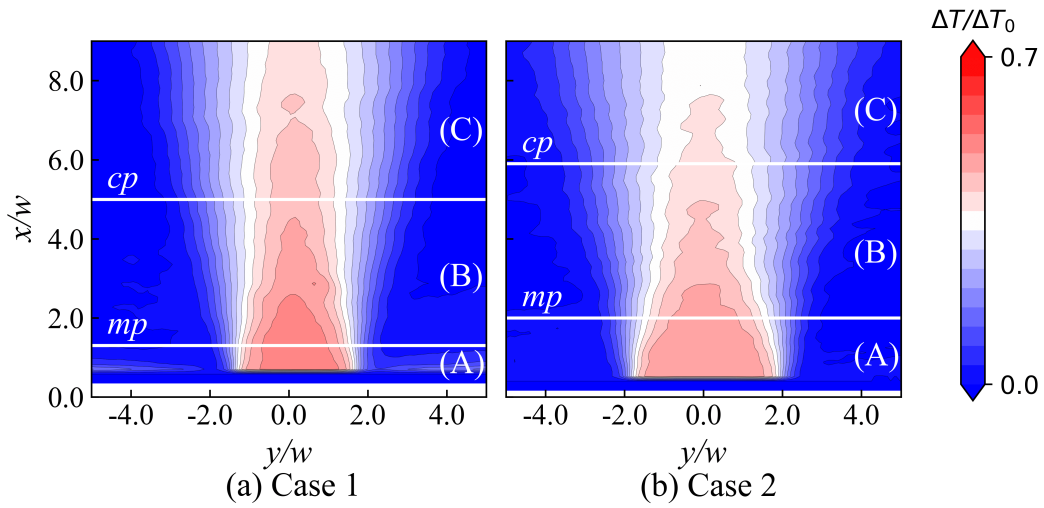


Figure 5. Dimensionless temperature differences between jet and surrounding fluid for (a) case 1 and (b) case 2.

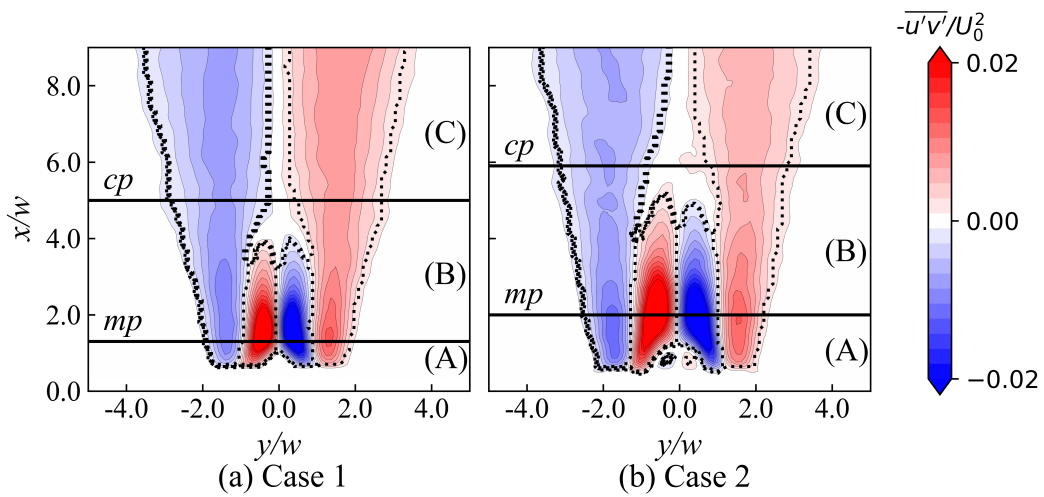


Figure 6. Dimensionless mean Reynolds shear stress for both cases with contour lines around shear layers for (a) case 1 and (b) case 2.

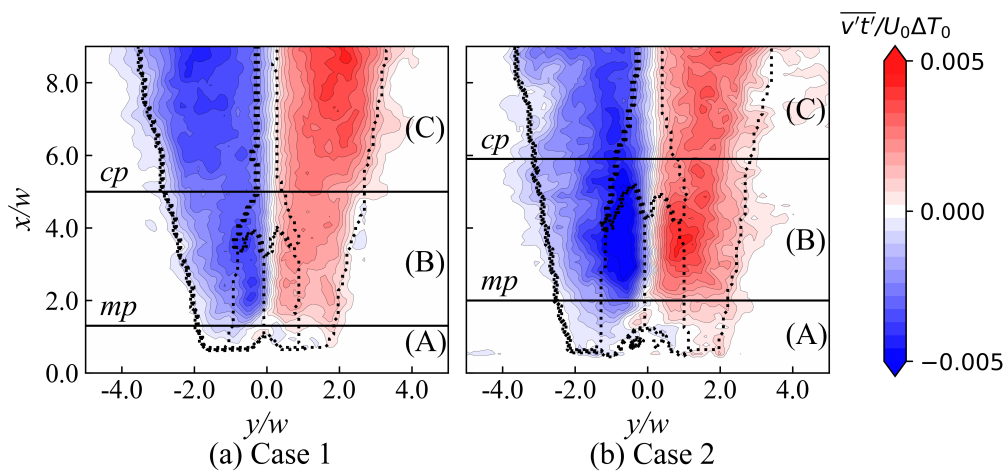


Figure 7. Dimensionless mean turbulent heat flux for both cases with contour lines around shear layers for (a) case 1 and (b) case 2.

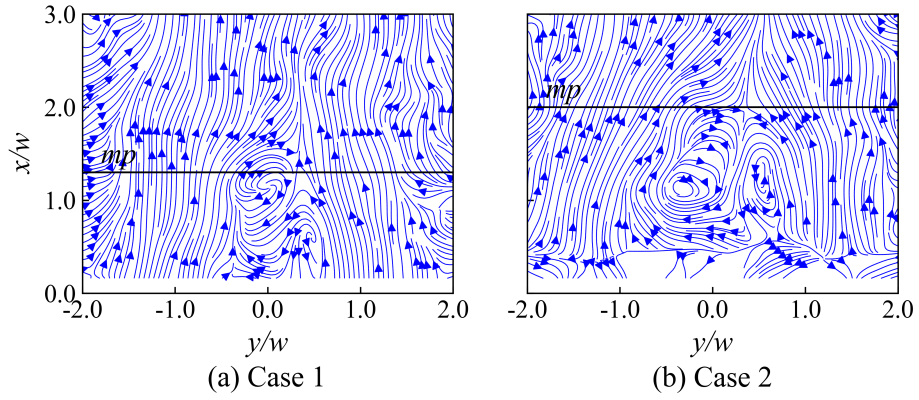


Figure 8. Instantaneous streamlines of the upstream region for (a) case 1 and (b) case 2.

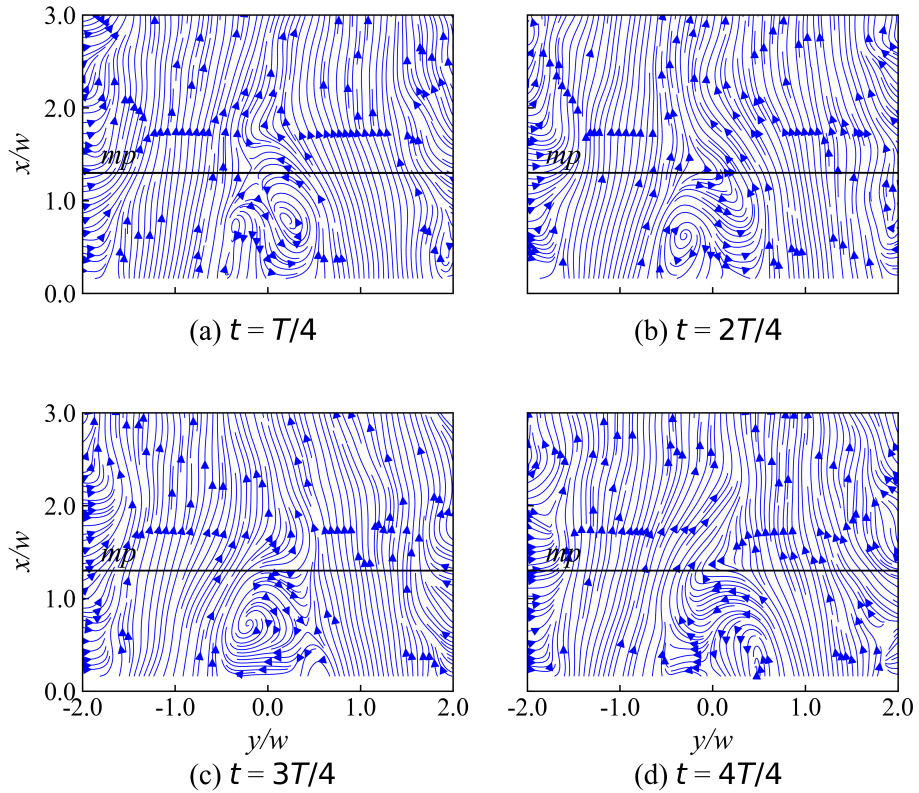


Figure 9. Phase averaged streamlines for case 1 within a time duration of T divided into four phases at (a) $t = T/4$, (b) $t = 2T/4$, (c) $t = 3T/4$ and (d) $t = 4T/4$.

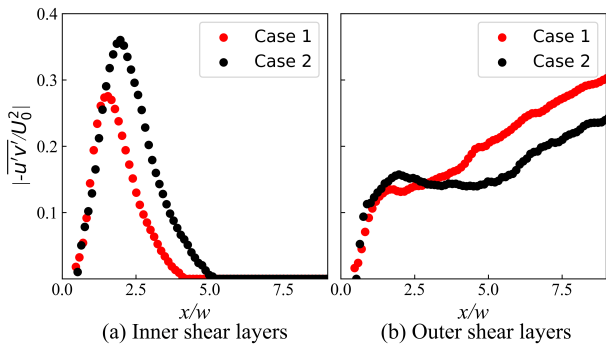


Figure 10. Total Reynolds shear stress across each cross-section for (a) inner shear layers and (b) outer shear layers.

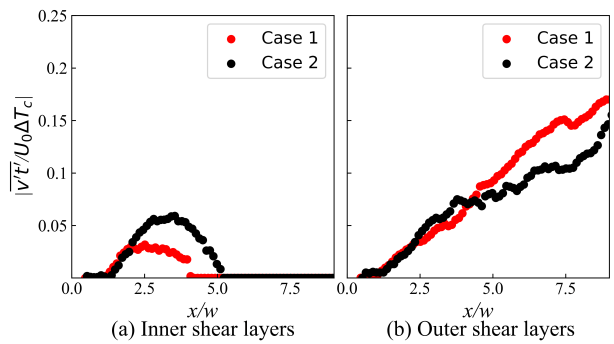


Figure 11. Total turbulent heat flux across each cross-section for (a) inner shear layers and (b) outer shear layers.